ROLL CONTROL VIA ACTIVE FLOW CONTROL: FROM CONCEPT DEVELOPMENT TO FLIGHT

Seifert, A., David, S., Fono, I., Stalnov, O, and Dayan, I.
Faculty of Engineering, Tel Aviv University

Bauminger, S, Guedj, R, Chester, S. and Abershitz, A.
Israel Aerospace Industries

Paper presented at the 49th Israeli Conference on Aerospace Engineering

ABSTRACT

This paper describes a series of experiments that enabled a flight demonstration of roll-control without moving control surfaces. That goal was achieved using a wing with a part span Glauert type airfoil, characterized by an upper surface boundary layer separation from the two thirds chord location at all incidence angles. The flow over that region was proportionally controlled using zero-mass-flux unsteady Piezo-fluidic actuators. The control was applied to one wing at a time, resulting in gradual suppression of the boundary layer separation, increased lift and reduced drag, leading to a coordinated turning motion of the small electric drone. The extensive collaborative and multidisciplinary study, starting from actuator adaptation, airfoil integration and 2D wind tunnel tests led to the selection of a configuration for the flight demonstrator. Further development of a light-weight wing, Piezo-fluidic actuators along with a compact, light-weight, energy-efficient electronic drive-system was followed by full-scale wind tunnel tests and three successful flight-tests. It was flight-demonstrated that active flow control (AFC) can induce roll moments that are sufficient to control the vehicle flight path during cruise as well as during landing. These were, to the best of our knowledge, first time achievements that should pave the way to further integration of AFC methods in flight vehicles for hinge-less flight attitude and flight path control as well as improved performance and increased reliability with lower observability.

Background and motivation

Active flow control (AFC) of boundary layer separation is intensively studied at Tel Aviv University and elsewhere for more than three decades [1]. The delay of boundary layer separation is a high-risk high-payoff task, with studies that date back to the time Prandtl [2, 1904] who formulated the boundary layer equations and identified their failure due to boundary layer detachment. Prandtl also suggested a remedy, using steady suction and cylinder rotation to replace and/or re-energize the sluggish boundary layer flow. Steady-suction and wall-tangential blowing [in Lachmann, 1961] were intensively studied and even reached production airplanes, but were abandoned due to low efficiency, excessive weight, complexity and reliability concerns. Unsteady control of shear-layers has the potential of overcoming the efficiency barrier, provided that flow instability, rather than brute force is applied. Oster and Wygnanski (1982) provided a benchmark demonstration of forced excitation of *turbulent* shear layers for mixing enhancement. Enhanced mixing is the leading mechanism explaining the efficacy of AFC for boundary layer control (BLC) over aerodynamic surfaces. Early studies of active BLC focused on enhancing the lifting performance of rather benign airfoils such as the NACA 0012 and 0015 at low Reynolds numbers (below one million). Many published studies suffered from the complex interplay between transition promotion of *laminar* boundary layers (resulting in postponed separation) and the delay of *turbulent* boundary layer separation due to energized near wall fluid. The study of Seifert and Pack (1999) provided the first demonstration of active BLC at Reynolds number up to 30 millions, corresponding to transport planes at take-off. However, more recently it became apparent that active BLC can not increase the maximum lifting performance of well designed airfoils operating at their design point, at least before an engineering design tool that includes AFC would become available

[Collis et al, 2004]. This is because AFC was considered a retrofit rather than an integrated design capability in all known studies. Until such a design capability would be available, the technology could bring significant benefits in several other focal areas, such as:

1. Maintaining high-lift at low Reynolds numbers (below 100,000), where natural transition is absent,
2. Managing laminar and more importantly turbulent separated flows ("bubbles", "burst" vortices over delta wings),
3. Reattaching separated flows for generating control moments (Yom-Tov el al, 2003, 2005, Timor et al, 2007), and
4. Drag reduction of bluff bodies (open loop studies by Ben Hamou et al, 2007, Seifert et al, 2008).

The above mentioned applications are essentially the manifestations of the same mechanism, AFC applied over different geometries at different flow conditions to mitigate boundary layer separation.

The current effort falls into the 3rd category. By partially or fully reattaching the separated flow at the aft-upper region of a modified Gluaert type airfoil (Glauert, 1945, 1948, Seifert and Pack, 2002, Yom-Tov and Seifert, 2005) it is possible to significantly increase the lift and significantly reduce the drag over the entire relevant angles of attack range. Our concept is inherently different of other studies applying AFC to conventional airfoils (limited to post-stall or requiring intentionally separating the flow over sections of the airfoil). The current separation control approach could be achieved in a gradual manner, proportional to the magnitude of the control authority. By applying the AFC over segments of a finite span wing, it should be possible to generate sufficient roll-moments to control the roll-axis and roll-motions of an airplane while reducing the drag on the higher lift wing, resulting in proverse yaw. This is what the current study was designed to do, and was demonstrated in-flight for the first time.

DESCRIPTION OF THE R&D ACTIVITIES

A series of experiments were performed at the following locations and with the following goals in mind:

1. The actuator calibration lab at TAU was used for calibrating the actuator prototype, the actuators for the 2D tests and the actuators used for flight tests with the ground drive electronics as well as the custom-made light-weight flight drive electronics.
2. The Meadow-Knapp low speed wind tunnel at TAU was used for the 2D airfoil tests. Lift, moment and form-drag were calculated from surface pressures and drag was calculated by wake integration. A 21% thick, 275mm chord airfoil with a modified Glauert type airfoil (used before by Seifert and Pack, 2002 and by Yom-Tov and Seifert, 2005 but cropped at 0.95c) with Piezo-fluidic actuator array located at 67% of the chord was fabricated from fiber-glass epoxy skin and the aluminum made actuators were integrated in it.
3. Vehicle and wing design were performed. To save resources, an existing small electric drone was used. The wing was redesigned to allow increased airplane weight and lower stall-speed and the body was extended to allow storage of the actuators' drive electronics and integration with the vehicle control system.
4. The low speed wind tunnel (LSWT) at IAI was used to test the complete airplane just prior to flight tests. Baseline aerodynamic data as well as controlled data, using both a lab electric drive system and the flight drive system with its remote control capabilities were tested. These experiments were crucial in reducing the risks of the first flight test.
5. Three successful flight tests were conducted, including data acquisition from the drone telemetry system.

The following sub-sections of the paper describe each of the above defined tasks.

1. Development and testing of the light-weight actuators and flight drive system

The chord of the modified Glauert airfoil for the flight tests was chosen to be 275mm (similar to the existing drone wing chord), and with a thickness of 21%, that resulted from cropping the last 5% of the modified Glauert airfoil used previously, a significant internal volume became available. This was accompanied by a strict requirement for light weight and energy efficiency. The chosen technology for actuation was Piezo electric due to the compactness, low weight and superior energy efficiency of this actuation technology, as compared to any other known actuation concept (see Arwatz et al, 2008, for a discussion on the subject). The TAU made Piezo-fluidic actuators were proven to be very compact and robust (Yehoshua and Seifert, 2003) while consuming about 1 to 3 watts while operating at the Helmholtz resonance frequency and generating peak exit velocities in the order of 50m/s from a 1mm wide 40mm long slot. Figure 1 shows a cross section of the Glauert airfoil with the actuators installed. The total length of the actuator is less than 50 mm and its thickness is less than 7 mm. During the first generation 2D tests, the actuators were installed from the side and bolted to the fiberglass skin from the outside, but this was altered to be installed and bolted from the outside for the flight test wing (see Figure 2), due to the one-block structure of the wing. Each actuator was instrumented with two Piezo electric disks and had its own sealed cavity, open only to the external upper surface through a slot, 1 mm high and 40 mm wide. It can be appreciated from Fig. 1, that the slot ejected the ZMF excitation in a shallow downstream directed angle, as in all the previous studies on this type of geometry. The free-end of the actuator was supported by the main beam of the wing.
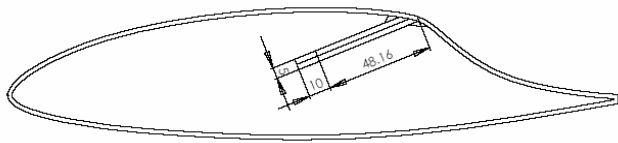
Figure 1: A cross-section of the modified Gluert airfoil. Chord is c=275 mm, its thickness is 21%. The actuators' exit slot is located at x/c=0.67, ejecting the ZMF excitation in a shallow downstream directed angle.


Figure 2: A rear-view of the airplane wing, the opening for the actuators and the actuators' exit slots before being installed in the wing. Twelve actuators were installed in each wing.

The prototype actuator (made by rapid prototyping technique) was bench-top tested for frequency and peak exit velocity, by placing a calibrated hot-wire (uncertainty of 2%) and measuring the peak exit slot velocity. It was found that the Helmholtz resonance frequency was about 1200Hz. An amplitude scan of the prototype actuator is shown in Figure 3a. The peak velocity curve shows the typical linear and then quadratic behavior of the peak velocity versus the excitation voltage, with the target of Up=40m/s reached at about 100 Vac. The right side ordinate, showing the power consumed by the actuator indicates that about 3 Watts are required for each actuator to generate the maximum desired fluidic excitation. This should bring the total power required for roll control close to 40 Watts. The weight of the prototype actuator unit was less than 30 g.

The performance of the actuator prototype deemed sufficient to freeze the design and to go ahead and integrate this design in the wing. For ease of assembly and integration it was decided to fabricate the actuators from aluminum at this stage.

While in laboratory experiments, the weight and power consumption of the drive electronics to operate the actuators is insignificant. However, it is crucial to minimize weight and power consumption of the flight actuator drive system. In addition, the drive system should be integrated with the drone remote control system, be immune to electromagnetic noise and not adversely affect the other components of the drone. Furthermore, it should be robust enough to withstand vibrations and landing impact.
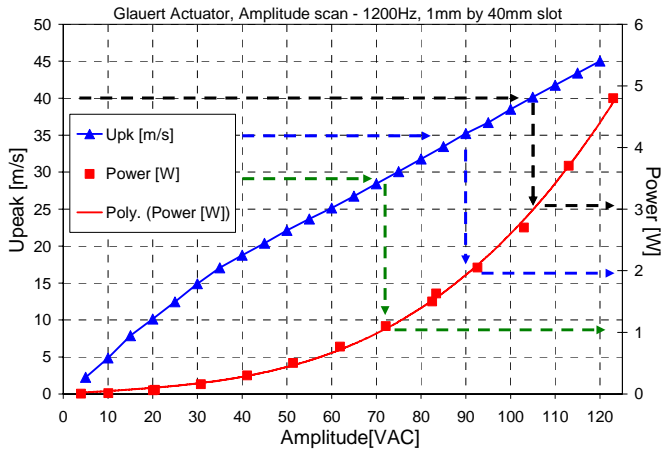
Figure 3a: An amplitude response test of the prototype actuator at the Helmholtz frequency, operated by the ground drive system. Left side ordinate shows the peak slot exit velocity and right side ordinate shows power consumption, both plotted against the input AC voltage.
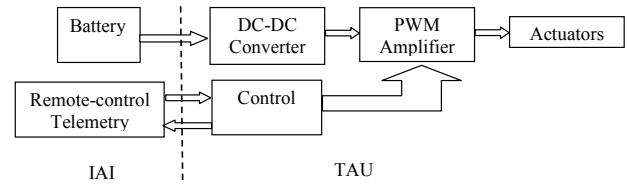
Figure 3b: Block diagram of the flight actuator drive system.

Figure 3b shows the block-diagram of the flight electronic drive system designed to operate the actuators in-flight and be operated via the remote control. The response of the actuators was desired to be proportional to the stick deflection, mimicking regular ailerons' operation. The flight electronic drive system was connected to the Remote Control (R/C) receiver as a standard servo channel. In *AFC flight mode*, the stick deflection was transmitted by the servo channel and, in turn, it modulated the pulse-width of a resonant DC-to-AC converter (DC-DC Converter with a PWM Amplifier). The output of the amplifier was band-pass filtered with an LC resonator, thus the voltage applied to the actuators was a sine-waveform at the actuator's Helmholtz resonance frequency (1400 Hz, increased from the about 1200Hz of the resin made actuator prototype) and the amplitude of the excitation signal was proportional to the stick deflection (in the range of 30 to 110 Vac). This voltage range was selected based on the aerodynamic response as will be shown in section 2 below. The excitation voltage was switched to the left or right wing actuators according to the direction of desired roll. The flight drive system was powered by the airplane's main battery at a nominal 16 Vdc. Due to the high efficiencies of the DC-DC converter and the PWM Amplifier, the overall power efficiency achieved was close to 90%. The dimensions of the flight electronic drive system were 8cm by 10cm by 24cm and it weights about 800 gm.

2. Two-dimensional airfoil experiments at Tel-Aviv University

Once the layout and design of the light-weight actuators was validated to provide the target performances during the bench-top tests, the airfoil for the 2D wind tunnel tests and the 12-actuators array was designed and fabricated. The airfoil was constructed from a 2 mm thick fiber-glass epoxy skin. Its chord was 275 mm and its span was equal to the tunnel's width, 609 mm. The model was instrumented with 31 pressure taps along its centerline and two additional rows of spanwise pressure taps, located at $x/c=0.1446$ and $x/c=0.8$. The 12 actuators-array was fabricated from aluminum, instrumented, bench-top tested and installed in the airfoil. The performance of the aluminum made actuators exceeded those of the rapid prototype actuator due to higher rigidity and tighter tolerances. The enhanced rigidity of the aluminum actuator resulted in an increase of the Helmoltz resonance frequency from 1200Hz to 1400Hz.

The performance of the actuators with the ground and flight drive electronics was tested and found to be identical, as shown by the amplitude scan of the peak excitation magnitude, presented in Fig. 4b.

4

After fabrication and actuator bench-top testing, the airfoil was installed in the 1.5m high, 0.609m wide test section of the Meadow-Knapp low speed wind tunnel at Tel Aviv University. First, the baseline performances of the 21% thick Glauert airfoil were tested, at the Reynolds number range intended for the flight tests (Re=280k-460k) with additional lower and higher Reynolds numbers for completeness.

The lift performances of the 2D Modified Glauert airfoil are presented in Fig. 4a.

Due to the massive flow separation from the aft upper surface of the airfoil (Fig. 1) at all incidence angles and the complex interplay between laminar-turbulent transition and boundary layer separation on such an airfoil at low Reynolds numbers, the baseline, clean airfoil, lift slope changes significantly at low incidence. As the Reynolds number increases, the lift slope becomes constant and the lift at low incidence increases. The maximum lift of the baseline – clean airfoil is about 1.25 and stall incidence is 18 degrees.

Following the studies of Seifert and Pack (1999) and Yom-Tov and Seifert (2005) it was expected that significant lift increment would be obtained at low and medium incidence angles when partial or complete flow reattachment would be affected by the fluidic excitation applied at x/c=0.67. Indeed, when the actuators were operated either in unison phase or π phase shift between every actuator pair (Fig. 5a), a significant lift increment was obtained. Note that at this excitation magnitude, the unison phase actuation results in smoother lift curve than the anti-phase (π) distribution, while the latter provides somewhat larger lift increment, as was previously noted by Seifert et al (1999) and Timor et al (2007).

A concomitant drag reduction is associated with the actuation, separation control and lift increment, as shown in Fig. 5b. The drag is essentially halved by the actuation. This is a desirable feature for roll control, since natural trimming will take place. When the lift will increase the drag will decrease so the nose will turn into the turning direction induced by the roll. On the other hand, undesirable and complex drag variations can be noted at low incidence. However, this behavior disappears at higher excitation magnitudes and tripped boundary layer conditions, as can be seen in Fig.7c.

These complex phenomena are accentuated when we consider the lift response to alternation of the excitation magnitude. The results shown in Fig. 6 present an almost step response (steady-state) of the lift increment to increasing the excitation magnitude. This response is highly undesirable since we are interested in a gradual response. It was again suspected that this response is due to the interplay between separation, transition and separation control. It is apparent that at higher incidence (Fig. 6, α=8°) and higher Reynolds numbers (not shown) the amplitude response of the lift is more gradual. This led us to force transition upstream of the actuation location. This was achieved by placing grit #60 on a 12mm wide double back tape (of thickness less than 0.1mm) at x/c=0.4. Indeed, the response of the rough airfoil to increase in the excitation magnitude became significantly more gradual (Fig. 6), though the lift increment was reduced. This is expected since forced transition just upstream of laminar separation (in natural flow conditions) delays boundary layer separation. However, the fact that the excitation is still effective and increases lift indicates that separation downstream of the actuator was not completely eliminated. The remaining potential lift increment, of 0.2 to 0.35, deemed sufficient for the purpose of the present test program. Since the response to excitation magnitudes that are lower than 30Vac was very weak, it was decided to set any deviation from neutral AFC "aileron" setting to 30vac.
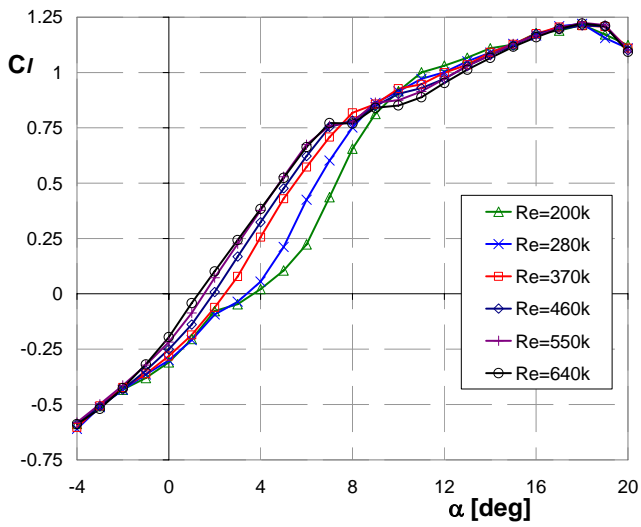
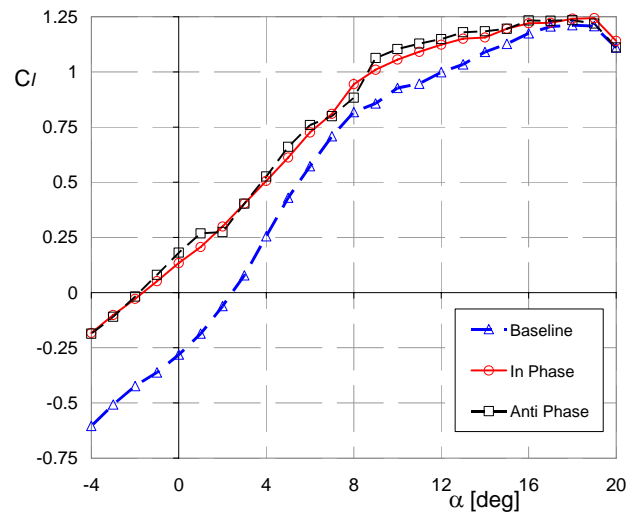**Fig. 4a: Reynolds number effect on the lift of the clean Modified Glauert airfoil performance, 2D TAU test.**

Fig. 5a: The effect of actuation on the lift vs incidence. Re=370k, Up=40m/s, forcing all actuators in phase and every other actuator phase inverted (termed "anti-phase". Triangles – baseline.
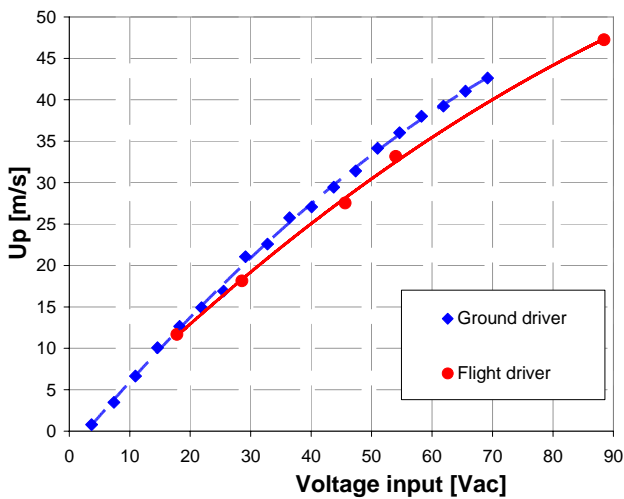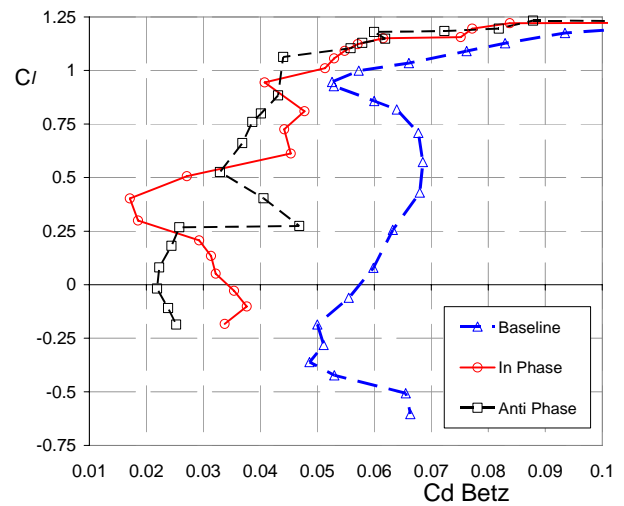

Fig. 4b: Amplitude response of the G275 airfoil actuators at 1380Hz, driven by the ground system (blue diamonds) and by the prototype of the flight drive system (circles). Obtaining about Up=40m/s consumed only about 2 Watts.
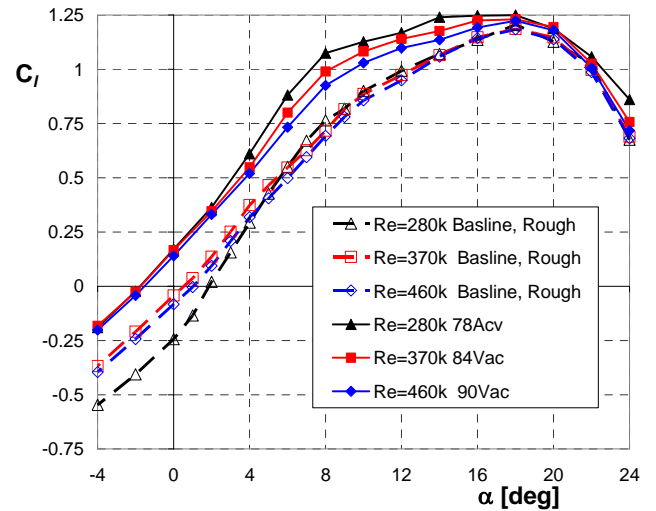

Fig. 5b: The effect of actuation on the lift vs drag. Re=370k, Up=40m/s, forcing all actuators in phase and every other actuator phase inverted. Triangles – baseline.
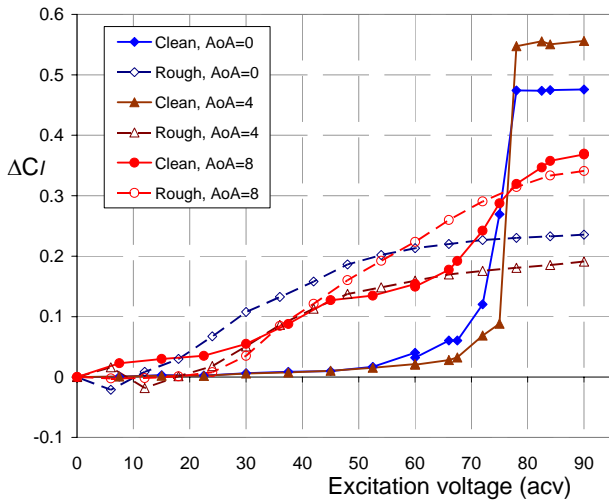
Fig. 6: Lift increment data versus the excitation magnitude at three angles of attack and Re=280k. Uniform phase. Smooth airfoil data: filled symbols, rough airfoil data empty symbols.

Fig. 7a: The lift performance of the baseline and controlled Glauert airfoil at the target Reynolds number range. Tripped boundery layer.

Figure 7a presents the baseline and controlled rough Glauert airfoil lift versus the airfoil incidence angle. The high sensitivity of the baseline to the Reynolds number (compare to Fig. 4a) is significantly reduced and a significant, though not constant, lift increment is available at all relevant incidence angles, with AFC activated. Note the different excitation magnitudes at the three Reynolds numbers, resulting in excitation momentum coefficients ($C_\mu \equiv \dfrac{hU_p^2}{cU_\infty^2}$) of 0.04, 0.025 and 0.018, at Re=280,000, 370,000 and 460,000, respectively.

The data also indicates a small lift increment even at the stall angle. The reduction of the Reynolds number sensitivity and the attainment of gradual lift increment at all incidence angles due to the actuation enabled us to proceed to the design of the wing and entire airplane for the full scale wind tunnel tests and for the flight tests.

The lift data shown in Figure 7b presents baseline and controlled 2D Glauert airfoil performances, as measured at TAU. The controlled data was acquired when the ground or the flight electric drive system operated the Piezo actuators array. All actuators were operated in unison, in order to simplify the electric drive system, although it was found that operation in "anti-phase" was more effective as well as significantly less noisy due to destructive interference of the generated noise. It can be noticed that the results of the actuation are identical regardless of the ground or flight excitation electronics. At this Reynolds number (the core of the velocity range of the planned flight tests) and with the roughness applied, an almost uniform lift increment of about 0.2-0.3 is obtained at incidence angles from -4 to 12 degrees and a smaller lift increment even at post stall incidence of 20 degrees. This is a highly desirable trend, allowing roll motion to be induced over the entire relevant incidence range.

Figure 7c shows the lift – drag polar of the 2D Glauert airfoil at TAU tunnel, for the baseline and the two actuation drive electronics. Again the results of the flight drive electronics are indistinguishable from the ground drive electronics. Note that the minimum drag is reduced from about 0.05 to about 0.03 with effective actuation and even at lift coefficient of 0.75 to 1 there is a 20% drag reduction with actuation. Further reduction is possible with alternating phase operation, requiring only minor additional development of the drive system.

Also note that the complexity of the drag behavior of the smooth 2D Glauert airfoil, identified in Fig.

7

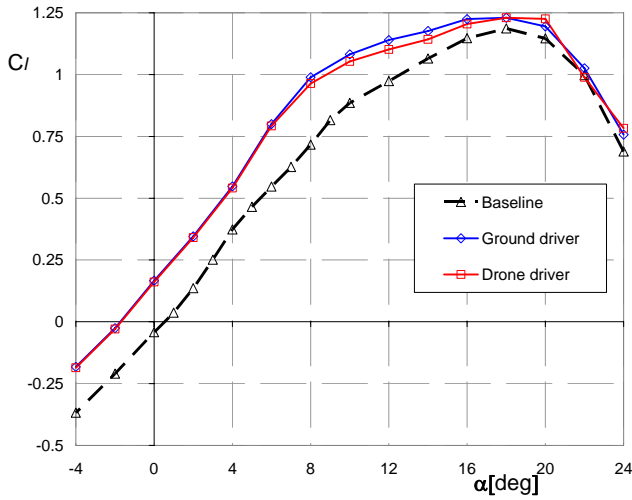5b, disappears with forced transition applied upstream of the actuation location, as shown in Fig. 7c.

Fig. 7b: Baseline and controlled lift vs incidence at Re=370k operated by the ground and flight drive systems. All actuators operate in unison, 85Vac, Up~45m/s.
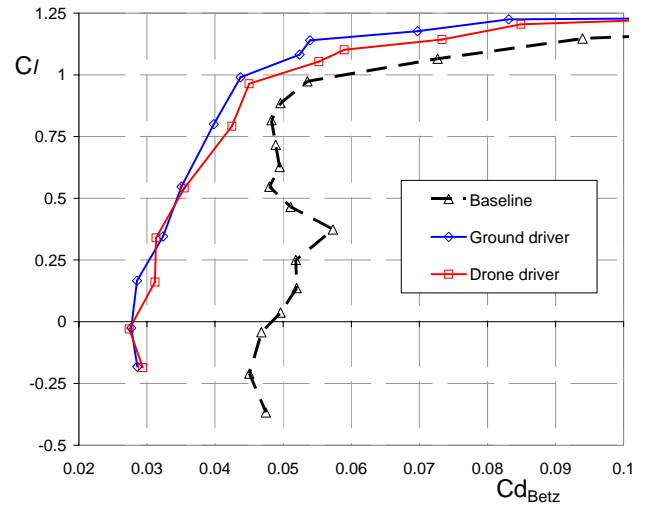
Fig. 7c: Baseline and controlled lift vs drag at Re=370k operated by the ground and flight drive systems, 85Vac, Up~45m/s.

3. Vehicle and wing design

The vehicle used for the flight tests is a modification of an existing IAI platform. It is an electric powered vehicle with an original maximum weight of 5kg and speed range of 20-40m/s. It can fly for about 1.5 hours. For the current project it was desired to increase the maximum weight to about 7.5kg and reduce the stall speed, to about 15m/s, for low speed AFC testing. For that purpose the new vehicle wing span was elongated to be 2.4m (from the original 1.8m span) while the chord was unchanged, c=0.275m. Figures 10 and 11 show the layout of the wing. The 30cm inboard from each wing tip are equipped with conventional ailerons. Next 60cm of the wing are composed of the Modified Glauert airfoil and equipped with 12 actuators array each. The central 60cm of the wing is of conventional airfoil and used to connect the wing to the body. Figure 8 shows a comparison of the Modified Glauert airfoil and the conventional airfoil contours. The conventional airfoil was designed with a similar lower surface contour to that of the Glauert airfoil, but with thickness ratio of 17.3%. Its maximum lift was computed to be about 0.15 higher than that of the Modified Glauert airfoil, while its drag was predicted to be much lower, about 0.0150 at conditions of Cl=0.8, Reynolds number of 300,000 and natural laminar case.
Figure 9 shows a rear-view of the wing with the Piezo fluidic actuators array exit slots shown. It was assured that smooth transition between the fiberglass and Aluminum parts was fabricated, to eliminate premature flow separations.
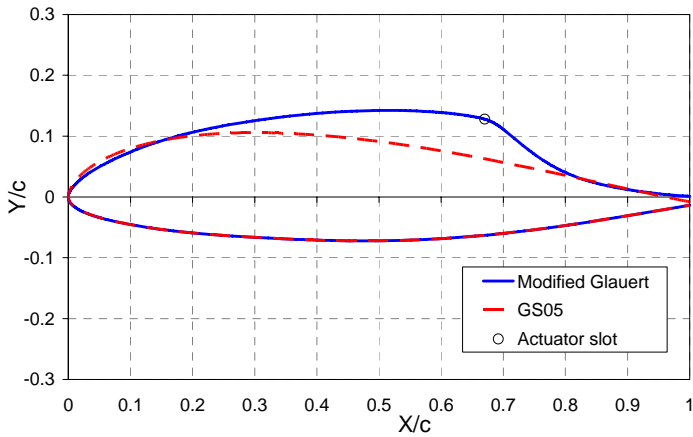
Figure 8: The Glauert and the conventional airfoil contours (used for the central region of the wing and for the wing tips) with a common lower surface. The circle on the Glauert airfoil contour indicates the actuator slot location.

Fig. 9: A rear view of the Gluaert section of the wing with the actuator exit slots. Each slot is 40 mm by 1 mm with 5 mm separating between each actuator pair. Twelve actuators array was installed in each wing.

Figure 10 presents the layout of the airplane with the AFC wing that is shown in Fig. 11. The central part of the body was elongated by 20cm (as seen in Fig. 12a) in order to accommodate additional equipment, such as the actuation drive electronics. The tail boom was elongated to increase the pitching moment of the tail. Details of the wing design could be seen in Fig. 11. End-plates were positioned between the Glauert and the conventional airfoil sections, since the upper surfaces geometry of the two airfoils are not identical (Fig. 8), in order to reduce 3D effects. Smooth fairing between the two sections could have been performed but was not done presently for fabrication cost savings.
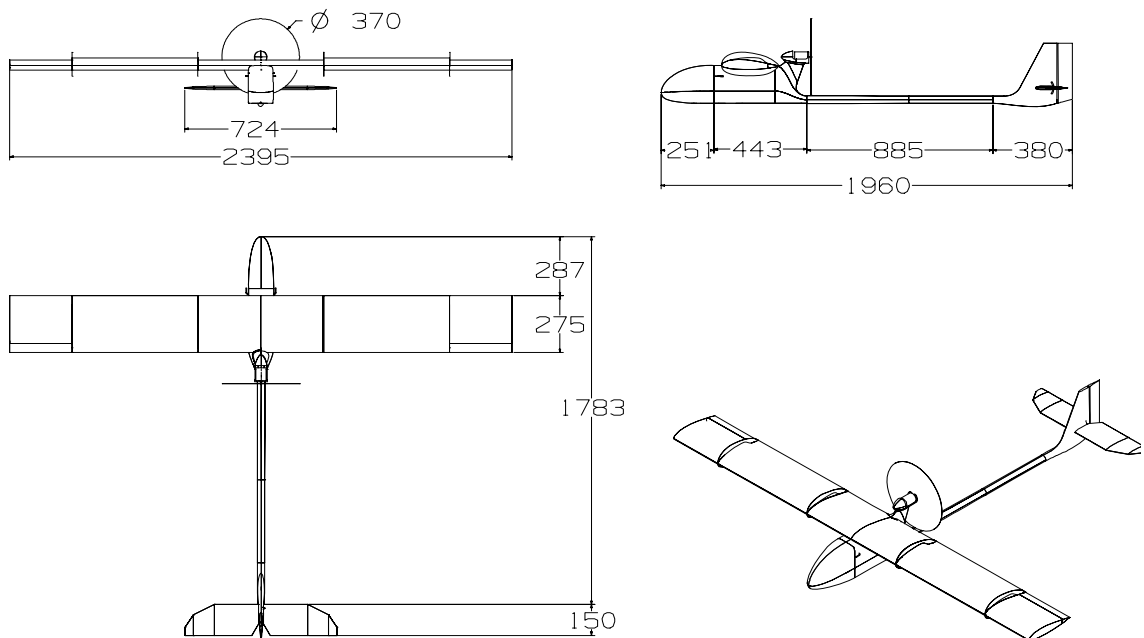
Fig. 10: The configuration of the flight demonstrator. Dimensions in mm. Wing surface 0.66m², wing incidence 3 deg at airplane zero incidence.
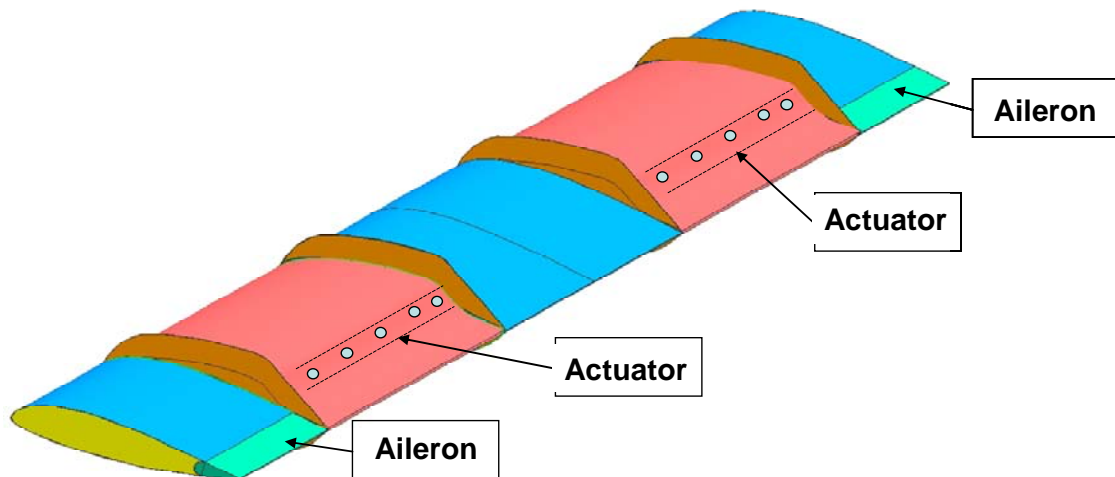
Fig. 11: The layout of the wing. The red sections are the Glauert AFC sections and the blue regions are the conventional airfoils. The conventional ailerons are shown at both wing tips, in green. The middle section and the Glauert sections are 600 mm each. The aileron sections are 300 mm each. The aileron is 20% of the chord. A switch on the remote control was used to alter the joystick purpose, from controlling the aileron deflection to controlling the AFC voltage to either right or left wings.

The total weight of the actuation system was about 1800gm, of which 500gm was the weight of each set of 12 actuators. The maximum power consumption of one actuator array (set of 12) was 45 Watts, including the drive electronics. With some additional refinements, the total weight of the actuators and flight drive system could be reduced by at least 50%.

4. Vehicle Low Speed Wind Tunnel tests

Full scale experiments at the planned flight Reynolds numbers range were performed on the flight-ready drone during a day and a half entry to the IAI low speed wind tunnel (LSWT). The test section dimensions are 2.4m high and 3.6m wide. The velocity range is 10 to 100m/s. The model was mounted on central bayonet and aft alpha rod. No image tests were performed. Figures 12a and 12b show photos of the drone installed in the test section of the IAI LSWT. The model was powered and some power runs were also performed to validate that sufficient thrust was available. When the motor was not operated, the pusher propeller was removed.
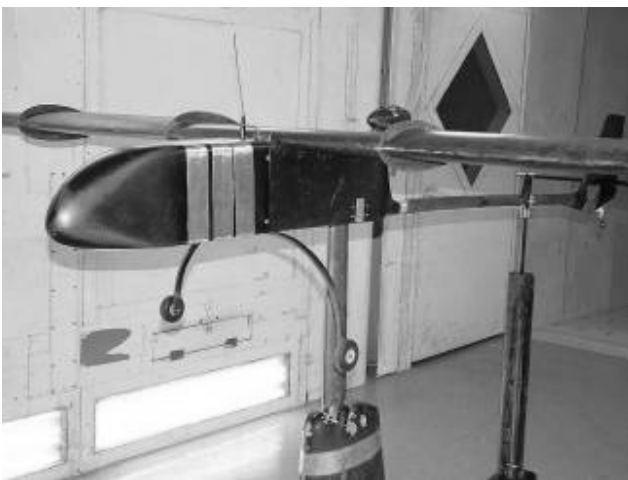
Fig. 12a: The airplane as installed at IAI LSWT.

Fig. 12b: The airplane as installed at IAI LSWT.

Figure 13 shows the lifting performance of the plane in the wind tunnel at a free-stream velocity of 20m/s. The maximum lift coefficient was found to be about 1.3 at about 15°, as expected from the 2D Glauert airfoil tests and the calculations of the conventional airfoil considering the 3° wing incidence at 0° airplane incidence. A desirable mild-stall was measured. Note that the lift slope of the blended airfoils wing is almost constant, a good trend compared to that of the 2D Glauert airfoil lift curve (Fig.7b).

Figure 14 shows the lift – drag polar of the airplane at a speed of 20m/s, corresponding to the main Reynolds number of 370,000. The minimum drag of the airplane is about 0.08 attributed to the body, engine nacelle, landing gear and the relatively high drag of the uncontrolled separations on the Glauert airfoil sections of the wing (about 0.05, as shown in Fig.7c, for half the span of the wing). Operating only one wing actuators increased the lift by about 0.1 and reduced the drag by 0.005 to 0.01 over most of the lift range. This would indicate a lift increment of about 0.3 and drag reduction of about 0.03 in the 2D Glauert airfoil equivalence, in good agreement with the 2D airfoil data shown in Figures 7a and 7b.

Figure 15 shows the airplane rolling moment due to activation of either wing actuators at a tunnel speed of 20m/s and 70-80Vac. The baseline rolling moment is not exactly zero since no effort was invested at trimming the plane in the tunnel prior to additional testing, due to time constraints. A rolling moment alternation due to actuation close to ±0.01, with respect to the baseline, can be noted over the entire incidence range. Of main concern is the proportionality of the resulting roll moments due to activation of the control input, i.e., the excitation voltage. The 2D Glauert airfoil tests have shown such a desired response, after the application of the roughness strip upstream of the actuators location (Fig. 6). A similar roughness strip with grit #60 was placed on the Glauert sections of the airplane wing, at 40%c, prior to testing and the roughness strip was left intact for the flight tests.

The data shown in Figure 16 indicates a gradual and desired trend of the rolling moment alternation due to increasing the voltage provided to the right wing actuators. A threshold of about 40Vac for the initial response of the rolling moment could be identified, in line with the data of Fig. 6, after the addition of the roughness to the wing. The response is close to being linear, a highly desired feature from the control point of view. Identifying the threshold of about 40Vac for the initial response to actuation, the same threshold level was used for setting the offset on the remote control for the control of supplied voltage during the flight tests.
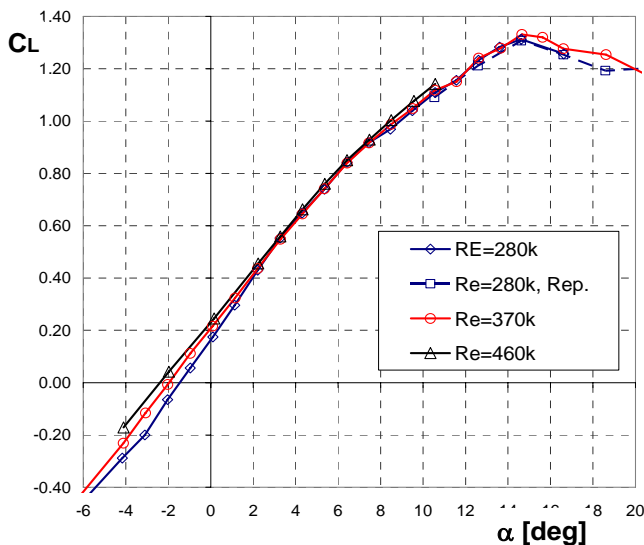

Fig. 13: The baseline lift of the plane, as measured at IAI LSWT, at the Reynolds number range corresponding to 15, 20 and 25m/s. Roughness strip installed.
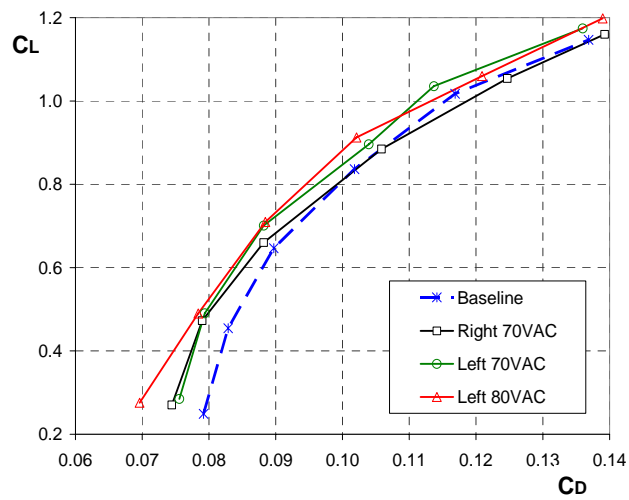
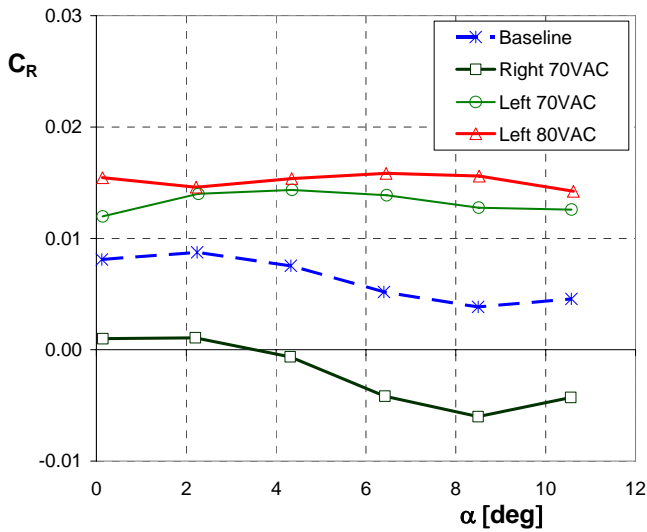**Fig. 14: Baseline and AFC controlled (one wing at a time) lift-drag polar.**

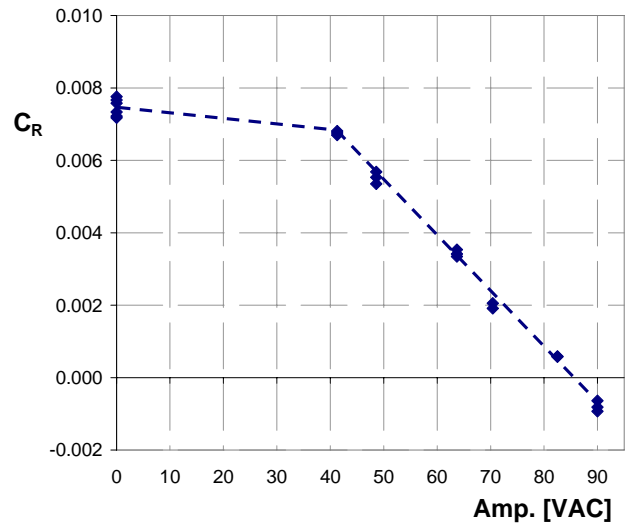**Fig. 15: Rolling moment vs airplane incidence with AFC applied either to the right or left wings. V=20m/s.**

Fig. 16: Airplane rolling moment vs AFC voltage applied to the right wing. α=2 deg, V=20m/s.
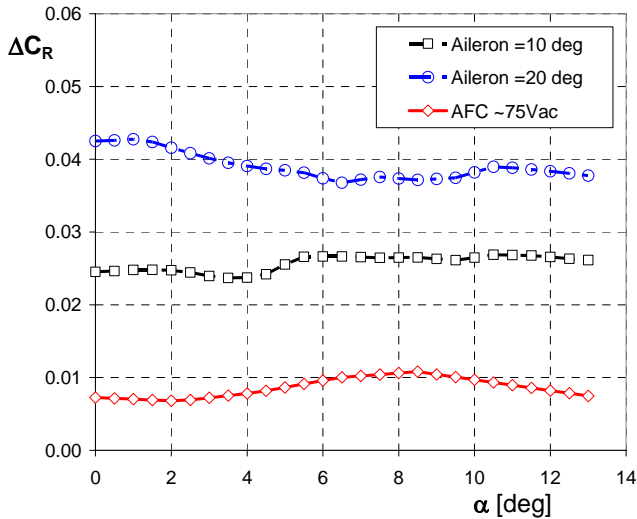

Fig. 17: A comparison of the rolling moment induced by conventional aileron deflections of 10 and 20 deg to activation of the one wing AFC at 70-80 vac (average of two wings) at V=20 m/s.
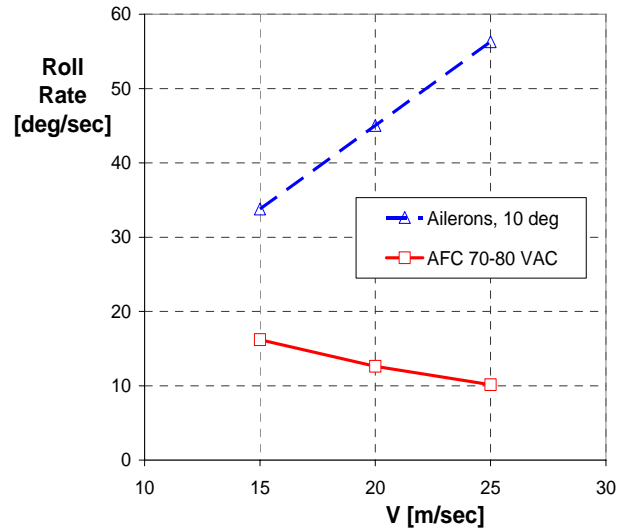

Fig. 18: A comparison between the expected roll rate between 10 deg aileron deflection and AFC induced roll (using 70-80Vac) at V=15-25 m/s flight speed.

The data shown in Fig. 17 presents the rolling moment control authority due to 10 and 20 deg aileron deflections compared to activation of the AFC on one wing (the data shown is averaged between two wings AFC operated at 70-80Vac with baseline Cr removed). An average rolling moment of 0.008-0.009 can be noted over the entire tested incidence range. This is comparable to an aileron deflection of 3-4 degrees according to the 10 deg aileron deflection data, or about a third of the control authority. It can be appreciated that the conventional ailerons start to lose effectiveness between 10 and 20 deg.

Figure 18 presents an estimation of the expected airplane maximum roll-rates based on the data of Fig. 17. The roll-rates were computed using steady roll rate equation, with damping roll coefficient, Clp, of 0.53. Note that the data for 25m/s is an extrapolation made on lower speed data. It can be seen that a factor of about 3 between the expected roll-rates based on the deflection of 10 deg ailerons versus activation of the AFC actuators at 70-80Vac is expected. Those rates will be compared to the flight test data, once processed. Also note the highly desirable trend of increasing the control authority of the AFC induced roll-rates as the flight speed decreases, while the conventional ailerons lose effectiveness. This

is because the fluidic excitation level was held fixed while the flight speed decreased, increasing the excitation momentum coefficient and also the control authority.

5. Flight tests

Following the IAI LSWT tests three flight tests were conducted, each lasting 10 to 15 minutes. Figure 19 shows the airplane ready for take-off at the airfield. The airplane behaved as expected with no surprises. Sufficient thrust was available and sufficient control authority in all axes was reported by the experienced pilot. Static stability was not an issue as well. According to the flight test data, the stall speed was below 14 m/s. Flight tests were initiated with a conventional controlled airplane configuration. At a safe altitude of several hundred feet, the flight control was switched to AFC ailerons and for about 5 minutes, during the first flight, the airplane was roll-controlled using *only* the AFC "ailerons". Figure 20 shows the roll command and resulting roll angle from the flight test data, acquired at 5Hz sampling rate and transmitted to the ground station. From t=1020 seconds and for about 5 minutes (3 mins are shown here) the data indicates regular and well-behaved flight path while roll was AFC controlled. The indicated airspeed for this segment of the flight was between 15 and 25m/s. Good tracking of the roll angle to the roll command can be identified. The pilot reported no special events but noted "a milder roll response by about a factor of three for a similar stick deflection" (without seeing the wind tunnel test results before!).

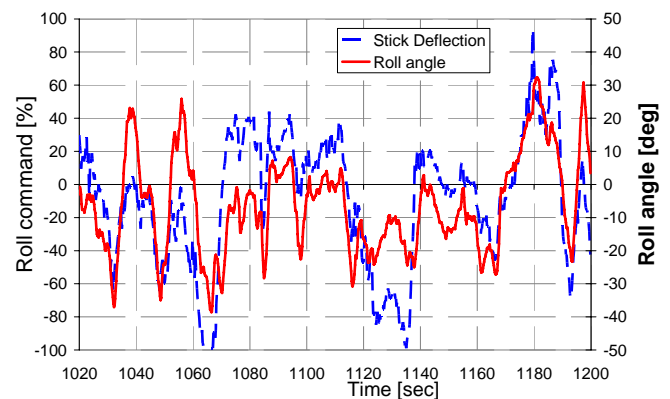Fig. 19: The airplane ready to be flight tested at the airfield.

Fig. 20: Flight test data showing the roll command (left side ordinate) and roll angle (right side ordinate) vs time. At 1200>t>1020 sec the roll control was induced *only* via AFC applied to either the right or left wings using the stick deflection.

During the 2nd flight test, several controlled maneuvers (doublets) were performed and the flight terminated with AFC-controlled *landing*. This was, to the best of our knowledge, one of the first times worldwide where AFC was flight demonstrated and certainly the *first AFC controlled landing*.

CONCLUSIONS AND RECOMMENDATIONS

An intensive design, development and test program, which took a fundamental active flow control concept from laboratory experiments to flight tests is reported. The purpose of the project was to demonstrate active flow control technology in flight and specifically to create roll motion without moving control surfaces. The chosen method was to manage the massive flow separation at the aft-upper region of a modified Glauert type airfoil. By installing an array of Piezo fluidic actuators slightly upstream of the baseline separation region it was demonstrated that significant and gradual lift and drag alternations are obtainable. A flight actuation system and its electric drive system were developed and

lab tested. A small electric airplane was modified to include two segments of the Glauert airfoil, one on the mid span region of each wing and of 25% the span each. Operation of the actuators on one side increased the lift and generated a gradual rolling moment, proportional to the applied voltage, as commanded by the stick deflection. Full-scale wind tunnel tests, validating the 2D wind tunnel test results, were followed by three successful flight tests. It included first time exclusive roll control via AFC and the first time landing with the AFC roll motion.

ACKNOWLEDGEMENTS

REFERENCES

1. Seifert, A., Darabi, A. and Wygnanski, I., 1996, "Delay of Airfoil Stall by Periodic Excitation", J. of Aircraft. Vol. 33, No. 4, pp. 691-699.

2. Prandtl L 1904 Uber Flussigkeits bewegung bei sehr kleiner Reibung. Verhaldlg III Int. Math. Kong. (Heidelberg: Teubner) pp 484–491; Also available in translation as: Motion of fluids with very little viscosity. NACA TM 452 (March 1928)

3. Lachmann G V 1961 Boundary-layer and flow control (Oxford: Pergamon) vol. 1 & 2

4. Collis, S.S., Joslin, R.D., Seifert, A. and Theofilis, V., "Issues in active flow control: theory, simulation and experiment", Prog. Aero Sci., V40, N4-5, May-July 2004 (previously AIAA paper 2002-3277).

5. Timor, I., Ben-Hamou, E., Guy, Y. and Seifert, A., "Maneuvering Aspects and 3D Effects of Active Airfoil Flow Control", (previously AIAA paper 2004-2614), special Issue of *Flow, Turbulence and Combustion* on "Air-jet actuators and their use for flow control", (2007), 78: 429-443.

6. Seifert, A., Bachar, T., Wygnanski, I., Kariv, A., Cohen, H. and Yoeli, R., "Application of Active Separation Control to a Small UAV", J. Aircraft, Vol. 36, No. 2, March-April 1999, pp. 474-477.

7. Yom-Tov, Y., Dabush, E., Belson, R. and Seifert, A., "Roll control of an MAV using active flow control, Paper presented at the 43rd Israeli Aerospace meeting., Feb. 2003.

8. Yom-Tov, Y. and Seifert, A., Multiple Actuators Flow Control over a Glauert type Airfoil at Low Reynolds Numbers, AIAA paper 2005-5389. June 2005.

9. Ben-Hamou, E., Arad, E. and Seifert, A., "Generic Transport Aft-Body Drag Reduction Using Active Flow Control", (previously AIAA paper 2004-2509), special Issue of Flow, Turbulence and Combustion on "Air-jet actuators and their use for flow control", (2007), 78: 365-382.

10. Seifert et al, "Heavy trucks drag reduction by active flow control", AIAA paper 2008-0743, Jan 2008.

11. Glauert, M. B., "The Design of Suction Aerofoils with a Very Large CL-Range", Aeronautical Research Council, R.&M. 2111, November 1945.

12. Glauert, M. B., Walker, W. S., Raymer, W. G., and Gregory, N., "Wind-Tunnel Tests on a Thick Suction Aerofoil with a Single Slot", Aeronautical Research Council R. & M. No. 2646, October 1948.

13. Seifert, A. and Pack, L.G. [C], "Active Control of Separated Flow on a Wall-mounted "Hump" at High Reynolds Numbers", AIAA J., V. 40, No. 7, July, 2002, pp. 1363-1372. (Part of AIAA paper 99-3430).

14. Rapoport, D., Fono, I., Cohen, K. and Seifert, A., "Closed-loop Vectoring Control of a Turbulent Jet Using Periodic Excitation", (AIAA paper 2002-3073), J. Propulsion and Power, V19, N4, Jul-Aug 2003, pp. 646-654.

15. Seifert, A., Greenblatt; D. and Wygnanski; I., "Aerial vehicle controlled and propelled by oscillatory momentum generators and method of flying a vehicle" (US Pat Appl. 20030229428, granted), June 2002.

16. Seifert, A., Eliahu, S., Greenblatt, D. and Wygnanski, I., 1998, "Use of Piezoelectric Actuators for Airfoil Separation Control (TN)", AIAA J., Vol. 36, No. 8, pp. 1535-1537.

17. Yehoshua, T. and Seifert, A. "Boundary Condition Effects on the Evolution of a Train of Vortex Pairs in Still Air", Accepted for publication, Aeronautical J., January 2006.